Title
INELASTIC SCATTERING OF l66-MeV O16 IONS BY Ta181

Authors
Isoya, A.
Conzett, H.E.
Hadjimichael, E.
et al.

Publication Date
1963-05-01

UCRL-10825

University of California

Ernest O. Lawrence Radiation Laboratory

INELASTIC SCATTERING OF 166-MeV O^{16} IONS BY Ta^{181}

Berkeley, California

DISCLAIMER

Proceedings of the 3rd Conf. on Reactions Between Complex Nuclei - Apr. 4-18, 1963

UCRL-10825

UNIVERSITY OF CALIFORNIA

Lawrence Radiation Laboratory
Berkeley, California

Contract No. W-7405-eng-48

INELASTIC SCATTERING OF 166-MeV O^{16} IONS BY Ta^{181}

A. Isoya, H. E. Conzett, E. Hadjimichael, and E. Shield

May 1963

INELASTIC SCATTERING OF 166-MeV O^{16} IONS BY Ta^{181}

A. Isoya†, H.E. Conzett, E. Hadjimichael, and E. Shield

Lawrence Radiation Laboratory
University of California
Berkeley, California

1. INTRODUCTION

Heavy ion elastic scattering data at energies above 100 MeV[1-3] have, generally, been subject to question with respect to the relative contribution of inelastic events leading to the lowest excited states of the target nucleus. Except for instances where light nuclei or Pb^{208} were the targets, such inelastic events could not be resolved from the elastic events with the experimental techniques employed. Analyses of these elastic scattering data have provided excellent theoretical fits and, thus, lead to quite precise determinations of nuclear absorption radii and surface thicknesses[1-3], or the equivalent optical potential parameters[4]. Hence, the question of the precision of the data becomes important. In general, we have been able to separate, in pulse-height spectra, those inelastic events associated with states of 1 MeV or more excitation by using a standard elastic peak shape determined at the smallest scattering angles. Inelastic events leading to lower lying states could not be separated in this manner. We have, therefore, in another experiment determined the combined yield for inelastic scattering of

166 MeV O^{16} ions to the lowest states of Ta^{181} at several (C.M.) scattering angles between 16 and 43 degrees.

In addition to measuring the previously unresolved inelastic contribution to our O^{16} + Ta elastic data, a second objective was to compare this determination with that calculated from Coulomb excitation theory[5] at scattering angles where the theory may be applicable; that is, at forward angles corresponding to (classical) trajectories of the O^{16} ions that do not pass through the nucleus, even though the incident ion energy is well above the Coulomb barrier. Since the inelastic scattering experiment reported here is considerably more difficult that that for elastic scattering, we consider this second objective to be the more important since it investigates the possibility of separating the major inelastic contribution to the elastic data by way of a straight forward calculation.

2. EXPERIMENTAL METHOD

In order to distinguish between inelastic and elastic events, coincidences between the scattered ions and the de-excitation γ rays from the lowest excited states were used. A 1-1/2 inch diameter by 1/4 inch NaI(Tl) crystal was placed with its axis normal to the scattering plane and as close as possible to the target, as shown in Fig. 1. This position of the crystal maximized the coincidence counting rate and minimized the error introduced by a possible non-isotropic γ ray angular distribution function. The γ ray background was reduced by providing a very well collimated beam from the heavy ion linear accelerator (Hilac) which passed cleanly through the target chamber,

striking only the thin target. The chamber with its particle and γ ray detectors was then completely enclosed with lead shielding. The background was then negligible compared to the γ ray yield from the target itself.

The level scheme of Ta^{181} (Fig. 2) [6] shows that a large fraction of the inelastic events corresponding to excitation of the ground state rotational band accompanies the 136-keV transition from the first excited to the ground state. Coulomb excitation of the higher states at 482 and 615-keV may be assumed to be much weaker than those to the ground state rotational band since their observed lifetimes are long compared to those of the lower states. Therefore, it is a good approximation to assume that the yield of the 136-keV transition measures the major contribution of Coulomb excitation to the inelastic scattering. Since the internal conversion coefficient of this transition is $\alpha = 1.7$, the observed 136-keV yield should be multiplied by a factor of 2.7 to obtain the total yield. For this energy the photo peak efficiency is quite high (~90%).

The γ ray detection efficiency as a function of energy is shown in Fig. 3. The chamber wall was made only thick enough to eliminate the x-ray background without too strong an absorption of the 136 keV γ rays. The absorption effect compensated somewhat the steep energy dependence of the NaI intrinsic efficiency so that the overall efficiency is peaked in the energy region of interest for this experiment.

A block diagram of the electronics used is shown in Fig. 4. The resolving time of the fast coincidence was set to 20ns., determined essentially by the rise time of the γ ray pulses (~ 10 ns) and the fine structure of the Hilac beam (at 70 Mc/sec, a pulse every

14 ns). Three energy spectra were recorded simultaneously: (1) the energy spectrum of the scattered ions, (2) that of the inelastically scattered ions in coincidence with γ rays ranging from approximately 80 to 180-keV, and (3) the spectrum of γ rays in coincidence with scattered ions corresponding to the "elastic" peak. A spectrum of these γ rays is shown in Fig. 5. Its shape did not depend sensitively on the scattering angle. The prominent peak was interpreted to be that of the 136-keV γ rays since it was expected that the excitation of the lowest rotational state would predominate, at least at forward angles. Fig. 6 shows spectra of the scattered ions taken at $\theta_L = 20^\circ$ in coincidence with γ rays selected (b) or not selected (c) in their pulse heights. The upper and lower levels of the pulse height selection are indicated in Fig. 5. The window accepted nearly all of the 136-keV γ rays, a considerable fraction of the 166-keV, and small fractions of possible higher energy gammas. It is seen that the inelastic particles detected in coincidence are well concentrated under the elastic peak. The peak widths are approximately the same as for the "elastic" peak (Fig. 6(a)); however, closer examination reveals that the low energy sides of the peaks seem to fall slightly slower than the high energy sides and the peak axes are shifted slightly (a few hundred keV) to a lower energy. The number the inelastic events without the γ ray pulse height selection (Fig. 6c) is ~~only~~ about twice that with it (Fig. 6b).[7] These observations do not seem to contradict the expectation that the intensity of the 136-keV de-excitation transition provides a measure of the inelastic scattering to levels lower than 1 MeV.

3. RESULTS AND DISCUSSIONS

Results of the measurements at various angles are shown in Table I. N^{peak} is the number of events in the elastic peak and $N_{(\gamma)}^{peak}$ is the corresponding number of inelastic events in coincidence with the selected γ-rays. Assuming that the inelastic scattering is represented by the intensity of the 136-keV de-excitation transition and that this γ-ray angular distribution is isotropic, the ratio $N_{(\gamma)}^{peak}/N^{peak}$ is related to the ratio, f, of the inelastic to elastic scattering recorded in the "elastic" peak as follows:

$$\frac{N(\gamma)^{peak}}{N^{peak}} = \frac{\Omega}{4\pi} \eta \, f/(\alpha + 1) , \qquad (1)$$

where Ω is the detector solid angle of the NaI crystal ($\Omega/4\pi = 0.22 \pm 0.04$), η is the γ ray counting efficiency (see. Fig. 3), and α is the conversion coefficient of the relevant γ rays ($\alpha = 1.7$).

Formula (1) is correct only when all the inelastic events occurring in the main peak correspond to excitation of the 136-keV state. However, the 136-keV γ-ray intensity is not strongly dependent on the relative population of the rotational levels. If the γ-ray pulse height selector accepted a considerable fraction of the 166-keV γ-rays, then formula (1) would give too high a value of f. Thus, if 77% of the inelastic events correspond to the first excited state and the rest to the second, as in the case of the E2 Coulomb excitation, the value of f obtained is too high by about 10%. If the first and second excited states have a comparable population, as may be the case in inelastic nuclear scattering, the value of f is about 24% too high.

Values of f are listed in Table 1 and plotted in Fig. 7 as a function of scattering angle. The curve expresses the sume of E2 Coulomb excitation probabilities for the first and second rotational excited states obtained from a semiclassical theoretical calculation[5] (Values of the parameters in our case: $\eta = 28.6$, $\xi = 0.01 \sim 0.03$). Two points at forward angles are very close to the theoretical curve, confirming the correctness of our assumptions. At higher angles f becomes a little less than the Coulomb excitation probability. Deviation from the curve starts at an angle of about $\theta_{c.m.} = 25$ degrees which corresponds to an angle just before the final rise in the curve of σ/σ_C vs angle.

In summary, we have found that Coulomb excitation of unresolved low lying states contributed as much as 5-8% to our "elastic" differential cross sections for 166-MeV O^{16} on Ta^{181} in the angular region before the sharp drop below the Rutherford values. Also, at backward angles where the elastic cross section falls well below the Rutherford value, the inelastic contribution was as large as 28%. Thus, precise analyses of heavy ion elastic scattering data can be meaningful only when the data have been corrected for such inelastic contributions. It appears that the calculated Coulomb excitation correction can be used over the range of angles where the theory is applicable.

ACKNOWLEDGMENTS

The authors wish to express their sincere thanks to the operating crew of the Hilac and to Mr. M. Nakamura and Mr. W. Goldsworthy for their advice and assistance with the electronics equipment.

REFERENCES

†Present address: Department of Physics, Kyushu University, Fukuoka, Japan.

1. J. Alster and H. E. Conzett, Proceedings of the Second Conference on Reactions between Complex Nuclei (John Wiley and Sons, Inc., New York, 1960); J. Alster, Thesis, UCRL-9650 (1961), unpublished.
2. H. L. Reynolds, E. Goldberg, and D. D. Kerlee, Phys. Rev. 119, 2009 (1960), Phys. Rev. 127, 1224 (1962) and references contained therein.
3. J. A. McIntyre, S. D. Baker, and K. H. Wang , Phys. Rev. 125, 584 (1962).
4. E. H. Auerbach and C. E. Porter, Paper A 3, this conference.
5. K. Alder, A. Bohr, T. Huus, B. Mottelson, and A. Winter, Rev. Mod. Phys. 28, 432 (1956).
6. Figure 2 shows only the lower members of the ground state rotational band and the 482-keV and 615-keV levels. Other low lying states are not Coulomb excited. See, for example, Nuclear Data Sheets (National Academy of Sciences, National Research Council, Washington, D.C.); B. Elbek, G. Igo, F. S. Stephens, Jr., and R. M. Diamond, Proceedings of the Second Conference on Reactions between Compled Nuclei (John Wiley and Sons, Inc., New York, 1960), p. 107; and A. H. Muir, Jr., and F. Boehm, Phys. Rev. 122, 1564 (1961).
7. In order to interprete the difference of the coincidence rates with and without the γ ray pulse height selection, one must take into account the fact that the internal conversion coefficient is small for the lowest energy γ rays so that the difference is enhanced. On the other hand the γ ray detection efficiency decreases gradually with increase in energy, resulting in the reverse effect for the higher energy γ rays. It is also possible that a considerable number of inelastic events that were in coincidence with the high energy γ rays may accompany γ rays of the lowest energy.

FIGURE CAPTIONS

Figure 1. Experimental apparatus.

Figure 2. Level scheme of Ta^{181}.

Figure 3. γ ray counting efficiency of the NaI detector as a function of the γ ray energy. η_0 is the intrinsic efficiency of the NaI crystal, $\exp(-\tau X)$ is the attenuation factor due to the absorption by the chamber wall, and thus $\eta_0 \exp(-\tau X)$ is an overall efficiency. A point on the curve of $\exp(-\tau X)$ is determined experimentally using a Co^{56} γ ray source.

Figure 4. Block diagram of the electronics.

Figure 5. A spectrum of γ rays in coincidence with the "elastically" scattered O^{16} ions at $\theta_L = 20^\circ$.

Figure 6. Spectra of O^{16} ions recorded at $\theta_L = 20^\circ$.

Figure 7. The ratio, f, of the inelastically to elastic scattering recorded in the "elastic" peak, as a function of scattering angle. Vertical bars on the points express the uncertainty in f due to that of the NaI detector solid angle. Horizontal bars express the angular range covered by the silicon detector aperture.

Table 1. Results of the measurements. The first and second columns give the mean scattering angle of the silicon detector in the laboratory and center-of-mass systems, respectively (the window of the detector subtended 5 degrees at the target). The third column gives the slow output pulse count N^{peak} of the silicon detector, which is nearly equal to the elastic peak area, as shown in Fig. 6a. The fourth is the inelastic scattering counts occurring in the elastic peak in coincidence with the selected γ ray pulse. The fifth is the corresponding accidental coincidence count determined from the independent measurements. The seventh is the fraction of inelastically scattered O^{16}-ions occurring in the elastic peak, calculated by formula (1).

θ_{Lab}	$\theta_{c.m.}$	N^{peak}	$N(\gamma)^{peak}$	N_{acc}^{peak}	$\frac{N(\gamma)^{peak} - N_{acc}^{peak}}{N^{peak}}$	f
15	16.3	267×10^3	201	115	0.32×10^{-3}	0.78×10^{-2}
20	21.7	558×10^3	745	128	1.11×10^{-3}	2.72×10^{-2}
		$1,130 \times 10^3$	1840	654	1.05×10^{-3}	2.60×10^{-2}
25	27.2	54×10^3	125	23	1.9×10^{-3}	4.6×10^{-2}
30	32.6	97×10^3	392	100	3.0×10^{-3}	7.4×10^{-2}
		88×10^3	355	55	3.5×10^{-3}	8.6×10^{-2}
		281×10^3	1095	174	3.25×10^{-3}	8.0×10^{-2}
35	37.9	20.1×10^3	148	12	6.8×10^{-3}	16.6×10^{-2}
40	42.9	3.1×10^3	37	2	11.0×10^{-3}	28.0×10^{-2}

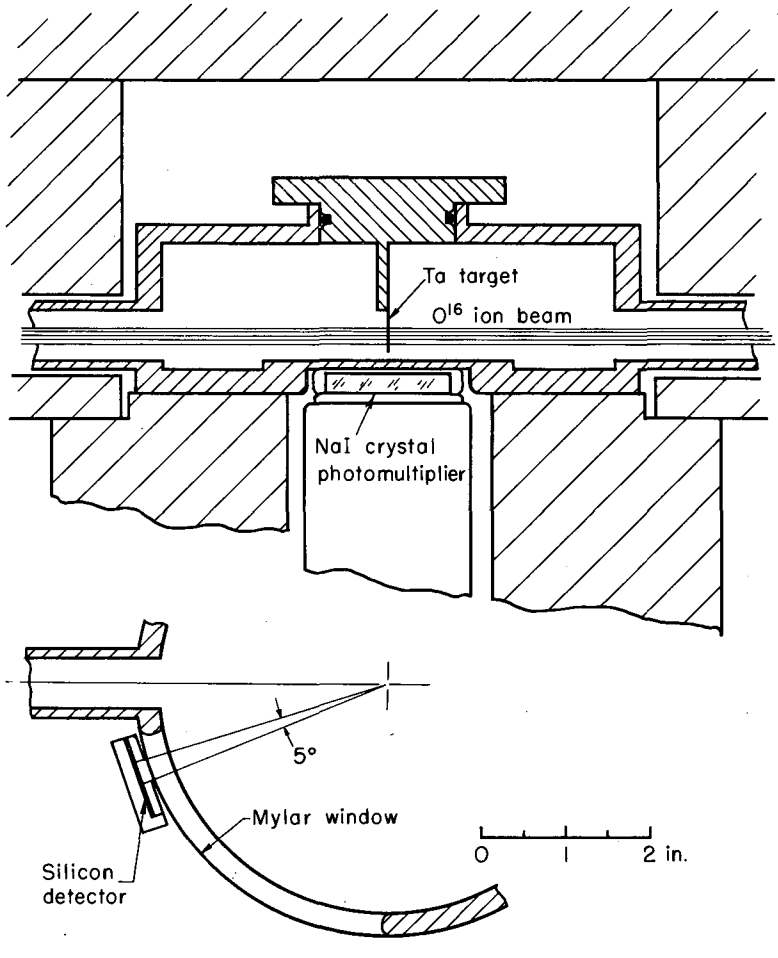
Ta target
O16 ion beam
NaI crystal
photomultiplier
5°
Mylar window
Silicon
detector
0
1
2 in.
MU-29994

Fig. 1.

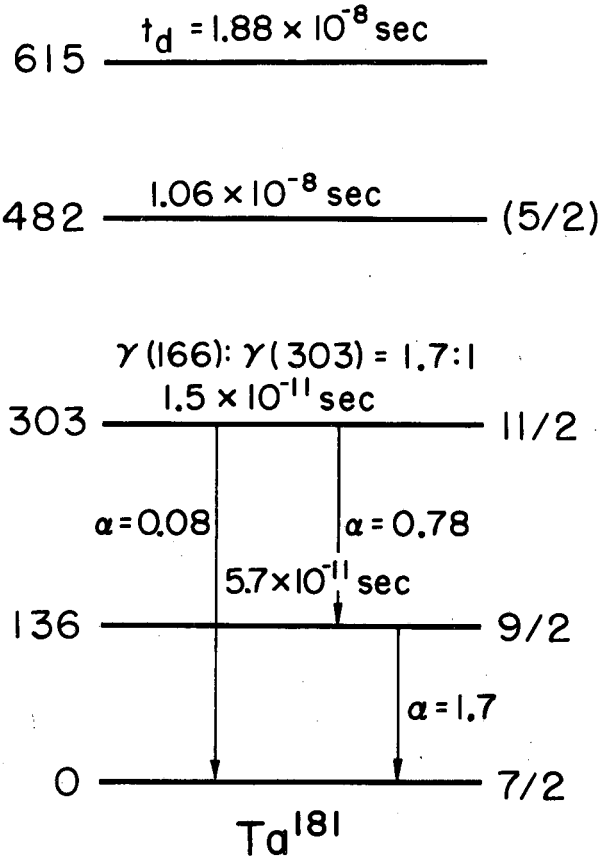

MU-29988

Fig. 2.

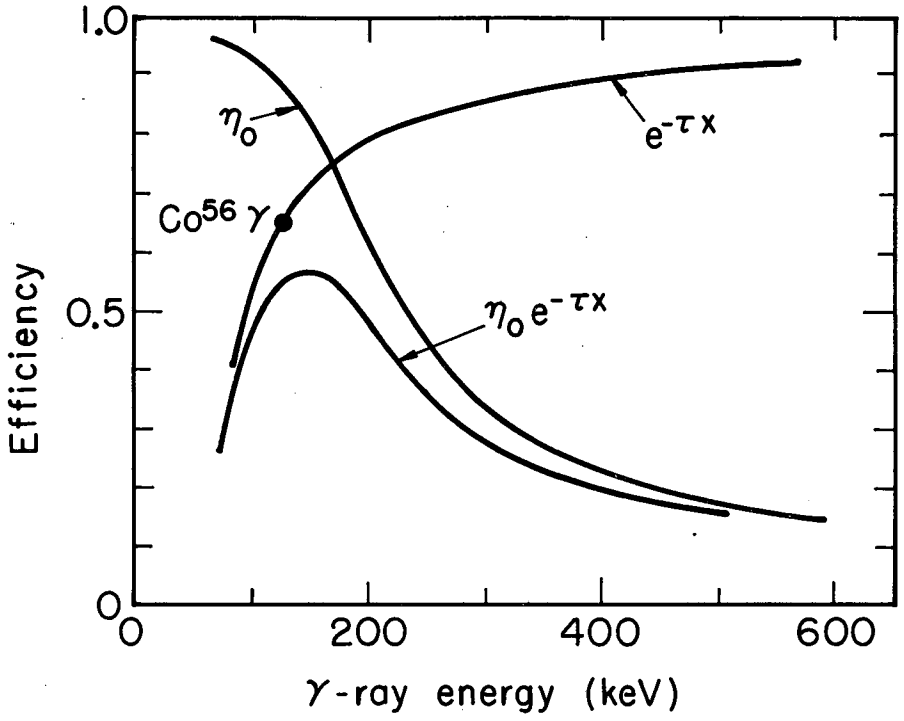

MU-29991

Fig. 3.

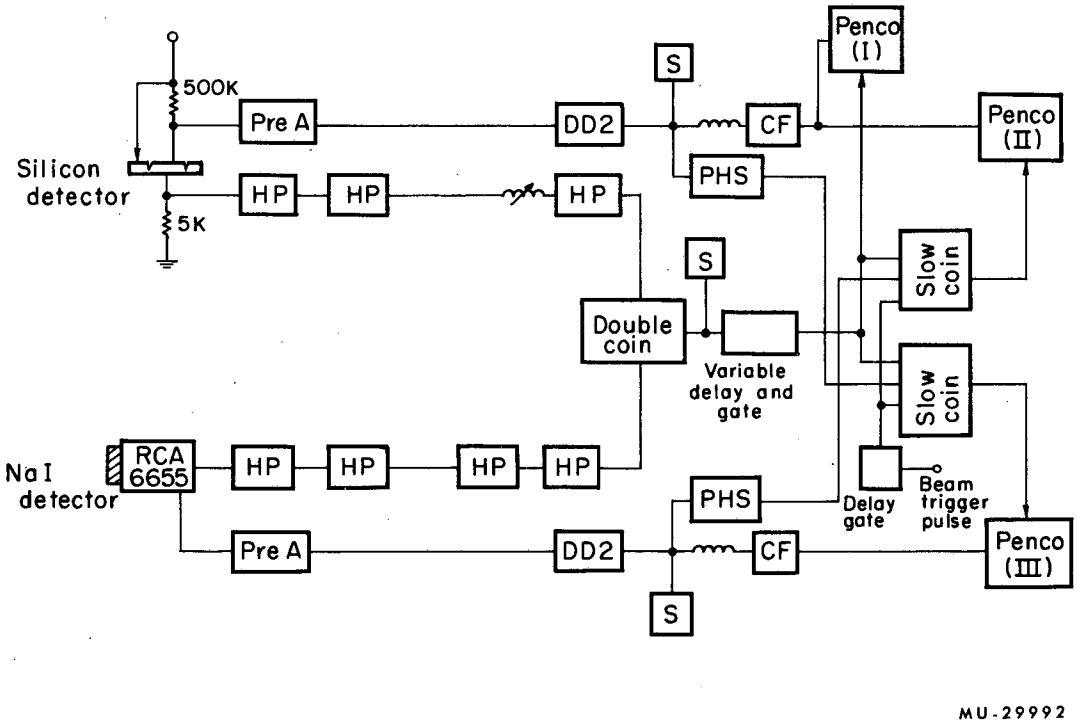
500K
Pre A
DD2
S
CF
Penco (I)
Penco (II)
Silicon detector
HP
HP
HP
PHS
5K
S
Slow coin
Double coin
Variable delay and gate
Slow coin
NaI detector
RCA 6655
HP
HP
HP
HP
PHS
Delay gate
Beam trigger pulse
Pre A
DD2
CF
Penco (III)
S
MU-29992

Fig. 4.

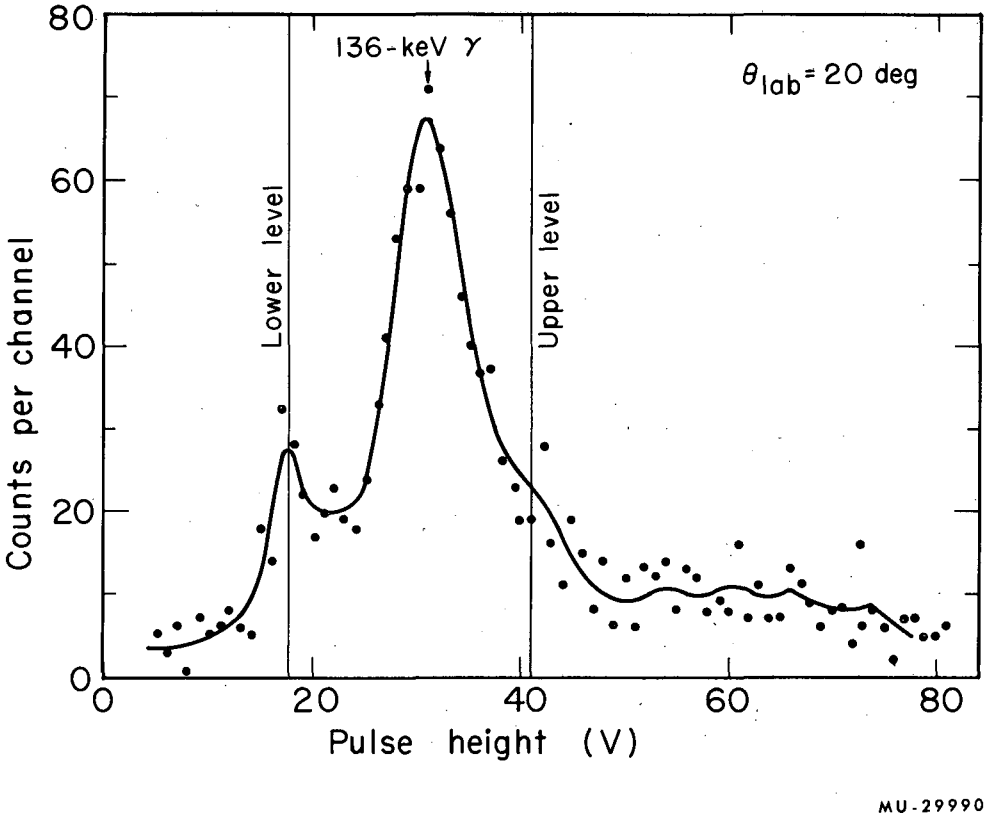
136-keV γ
θ_{lab} = 20 deg
Lower level
Upper level
Counts per channel
Pulse height (V)
0
20
40
60
80
MU-29990

Fig. 5.

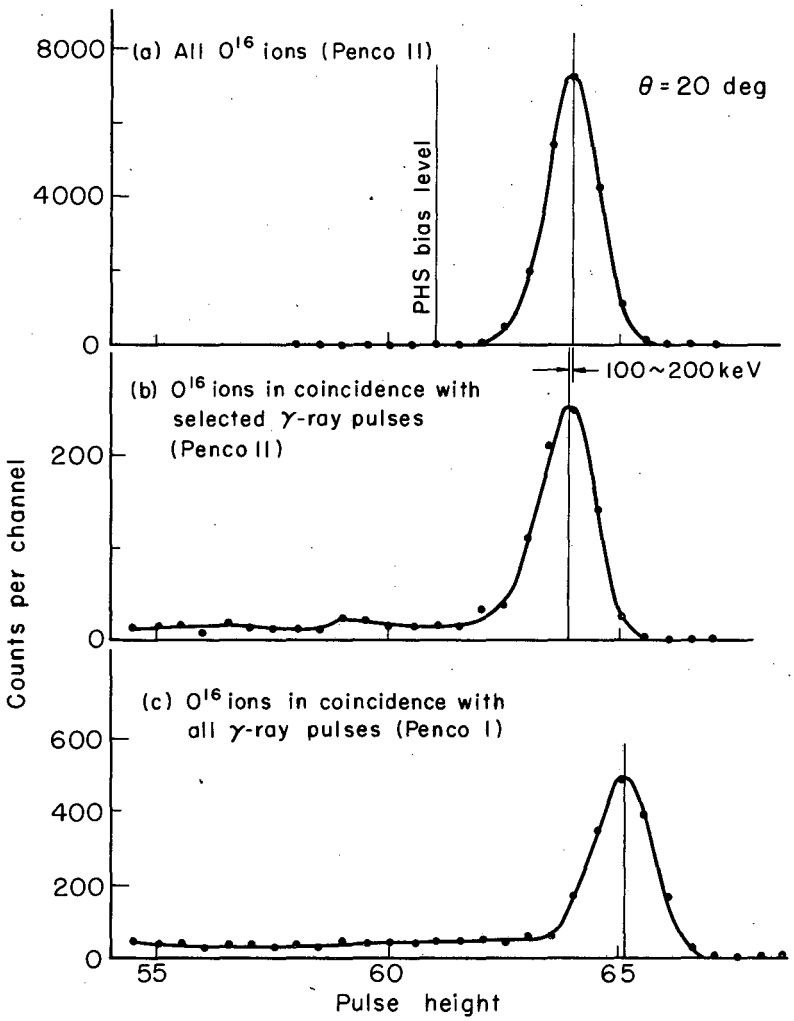
8000
4000
0
(a) All O^{16} ions (Penco II)
θ = 20 deg
PHS bias level
100~200 keV
(b) O^{16} ions in coincidence with selected γ-ray pulses (Penco II)
200
0
(c) O^{16} ions in coincidence with all γ-ray pulses (Penco I)
600
400
200
0
Counts per channel
55
60
65
Pulse height
MU-29993

Fig. 6.

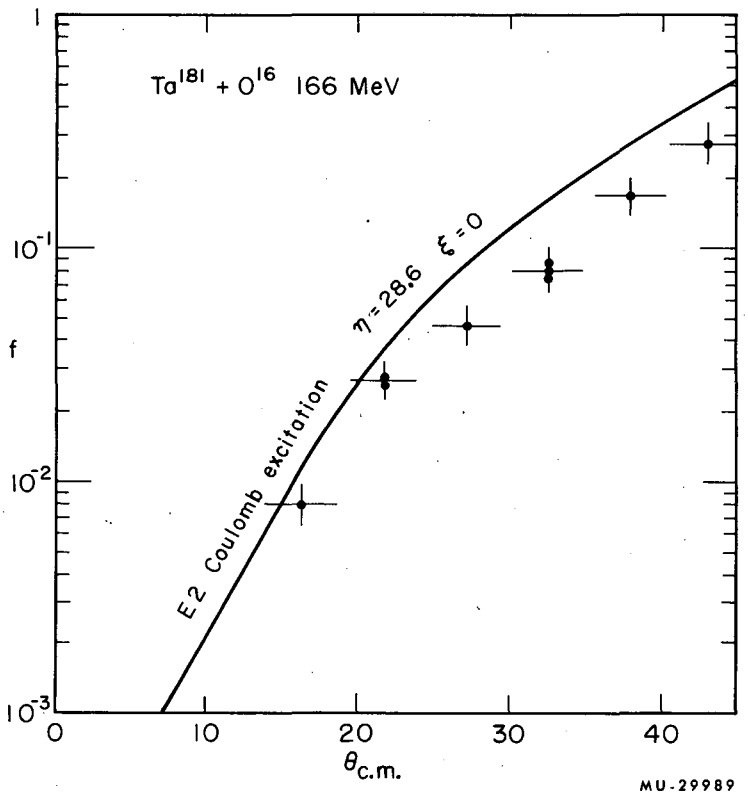
Ta181 + O16 166 MeV
η=28.6 ξ=0
E2 Coulomb excitation
f
1
10-1
10-2
10-3
0
10
20
30
40
θc.m.
MU-29989

Fig. 7.